LAWRENCE
LIVERMORE
NATIONAL
LABORATORY

LLNL-JRNL-673988

# Measurement of optical scattered power from laser-induced shallow pits on silica

E. Feigenbaum, N. Nielsen, M. J. Matthews

July 2, 2015

Applied Optics

## Disclaimer

# Measurement of optical scattered power from laser-induced shallow pits on silica

**Eyal Feigenbaum*, Norman Nielsen, and Manyalibo J. Matthews**

National Ignition Facility and Photon Science, Lawrence Livermore National Laboratory, 7000 East Ave., Livermore, CA 94550, USA
*Corresponding author: eyal@llnl.gov

**Abstract:** A model describing the far-field scattered power and irradiance by a silica glass slab with a shallow-pitted exit surface is experimentally validated. The comparison to the model is performed using a precisely micro-machined ensemble of ~11 μm wide laser ablated shallow pits producing 1% of the incident beam scatter in 10 mrad angle. A series of samples with damage initiations and laser-induced shallow pits resulting from 351 nm, 5 ns pulsed laser cleaning of metal micro-particles at different fluences between 2 J/cm$^2$ and 11 J/cm$^2$ are characterized as well and found in a good agreement with model predictions.

**OCIS codes:** (140.3330) Laser damage; (140.3300) Laser beam shaping; (290.0290) Scattering; (240.3695) Linear and nonlinear light scattering from surfaces; (240.6700) Surfaces;

## 1. Introduction

Mitigation of laser-induced artifacts on optics in high energy pulsed laser systems is central for extending the lifetime of these systems, for optimizing their performance, and for preventing potential damage from stray light [1,2]. Most of the previously reported characterization and mitigation efforts have been aimed at damage sites larger than a few tens of microns in depth with complex fracture-dominated morphologies. The reduction of their initiation can be achieved by optimized HF etching of the parts [3] and the mitigation of their growth can be achieved by controlled laser ablation [4,5]. However, this study is focused on much shallower pits that appear in greater densities, do not change morphology under subsequent laser pulses (i.e. no growth), and might cause power scattering performance reduction. Recently, we have reported laser-induced shallow pits (LSPs) on the exit surface of silica optics that are highly axisymmetric with a Gaussian-like profile, which are shallower but at relatively large numbers

with respect to the prototypical laser induced damage sites [6]. These LSPs are similar to those reported in the literature associated with the laser induced ejection of debris [7,8,9]. The evaluation of the resulting scattering is important, since it might lead to a reduction of power on target as well as unintended irradiation of other optics. The power scattering characteristics of shallow pits arrays is also useful for carefully designed morphologies that scatter coherent radiation into a radiation cone (e.g., the structure suggested at [10]).

Without a more informed method of relating the light scattering to the optical properties of these damage sites, one possible approach is to assume that all light that incident on their aperture will not reach the far-field, which will typically over-estimate their true power scatter contribution. Another possible approach could be the use of the optical surface roughness in combination with micro-roughness scattering methods [11-13]. Nevertheless, the specific and smoothly varying morphology of the LSP justifies a more informed analysis.

Recently, we have reported a model that links the LSPs morphologies to the resulting far-field scattered power [6]. The model yields relatively simple expressions for the scattered angle and the total scattered power given the nearly Gaussian-shaped LSPs width and depth. Here, we bring an experimental validation of the model based on a silica surface patterned with a controlled ensemble of similar shallow pits micro-machined (M-M) by laser ablation [4,5]. We then further investigate the morphology-scattered power relations for LSP ensembles on silica samples created by different pulsed laser fluences incident on surface bound particles and find a good match to model predictions.

## 2. Model for the scattered power model from LSPs

The model for scattered laser power from LSPs assumes a Gaussian profile and using far-field Fourier analysis and some algebra results in expressions for the far-field distribution and total scattered power [6]. The results of the model were verified with full electromagnetic numerical simulation. In this section we will review the main results of the model.

The electric field of the scattered light from a Gaussian shaped LSP with maximal depth of *h* and standard deviation $\sigma$ is:

$$E_{FF} = A_{NF} \sum_{m=1}^{\infty} \frac{i^m \cdot OPD^m \cdot \sigma^2}{\gamma \cdot m \cdot m!} \cdot \exp\left( -\frac{\sigma^2}{\gamma^2 \cdot m} \cdot r^2 \right) \qquad (1)$$

where, $A_{NF}$ is the near field amplitude of the incident wave, *OPD* is the maximal optical path difference: $OPD = -2\pi \cdot \Delta n \cdot h / \lambda$ , $\lambda$ is the free-space wavelength, $\Delta n$ is the absolute value of the

refractive index difference between the substrate and surrounding media (air), $\gamma = \lambda z / \pi$, $z$ is the propagation distance off the exit surface, and $r$ is the radial transversal coordinate. We find that the effective series with $m$<10 is a sufficient far-field representation for most of the typical LSP shapes found on exit surface of contamination-driven ablation.

The first term in the far-field series representation captures well the lower moments of the field distribution, and allows for a simple evaluator of the scattered light cone angle:

$$\theta_{FF} \sim \frac{\lambda}{\pi \cdot \sigma} \tag{2}$$

This angle increases with decreasing LSP width, but is independent of its depth. The maximal intensity, based on the first term, is proportional to $I_{FF} \propto h^2 \cdot \sigma^4$ , which can be correlated to the Rayleigh-Gans scattering intensity which is also proportional to the particle volume squared [11]. This observation highlights that the widest and deepest LSPs in the ensemble are more likely to dominate the total far-field intensity distribution.

Based on the spatial integration of the intensity of the field described in Eq. (1) and some algebra, the expression for the scattered power is:

$$P^{scat} = \left( \eta \left| A_{NF} \right|^2 \cdot \pi\sigma^2 \right) \left( \sum_{m=1}^{\infty} \sum_{l=1}^{\infty} \frac{i^m \cdot (-i)^l \cdot OPD^{m+l}}{(m+l) \cdot m! \cdot l!} \right) \tag{3}$$

where $\eta$ is the free-space wave impedance. The resulting scattered power expression could be interpreted as the incident power on $1\sigma$ area of the Gaussian phase object, i.e., $\pi\sigma^2$, (first RHS term in Eq. (3)) times the cross-section of the LSP ($\xi$) determined by its *OPD* (second RHS term). A 4th order polynomial is numerically fit to $\xi$ expression in Eq. (3) (for the range of depths smaller than 250 nm) and given by:

$$\xi \sim \left( -7.6 \times 10^{-11} \left[ nm^{-4} \right] h^2 - 1.8 \times 10^{-8} \left[ nm^{-3} \right] h + 4.2 \times 10^{-5} \left[ nm^{-2} \right] \right) \cdot h^2 \tag{4}$$

where $h$ is given in nanometers ($\xi$ is unit-less). Since the area that a LSP with a Gaussian phase profile covers is unbounded, and $\xi$ is defined in Eq. (3) with respect to a circle area of $\pi\sigma^2$, $\xi$

could exceed a value of one. For LSP depths substantially smaller than 1 μm the dominant term in Eq. (4) is the lowest order, resulting in a scattered power scaling of order $h^2$.

The net far-field intensity of an ensemble can now be evaluated based on the LSPs distribution. The net intensity of the ensemble is obtained as the incoherent addition of the individual LSPs intensities, justified by the large and aperiodic distances between the LSPs with respect to their widths. For LSPs with non-Gaussian profiles close agreement to model is obtained using an effective $\sigma$ ($\sigma_{eff}$) of a Gaussian shaped pit having the same volume as the examined LSP (where volume is defined by $V = 2\pi\int d(r)\cdot rdr$ , where *d(r)* is the depth profile).

## 3. Power scatter measurement

The scattered light around the optical axis from a pitted glass sample is characterized at the ultraviolet frequency range using the experimental setup illustrated in Fig. 1. The laser beam emitted from a ~5mW 351nm quasi-CW laser (CrystaLaser QUV-351-200) is spatially filtered and expanded using a typical pinhole arrangement to about a 2 cm diameter Gaussian beam spot on the sample. After the light passes through the sample it propagates to the far-field where it illuminates a Lambertian diffuse screen (Avian B250 - Barium Sulfate based coating). The scattered power is typically a fraction of a percent of the incident beam and therefore the diffuse surface has a center perforation that transmits the un-scattered beam to reduced backscattering. An ultraviolet sensitive CCD camera with programmable high speed electronic shutter (Spiricon SP620U) is used to image the far-field screen.

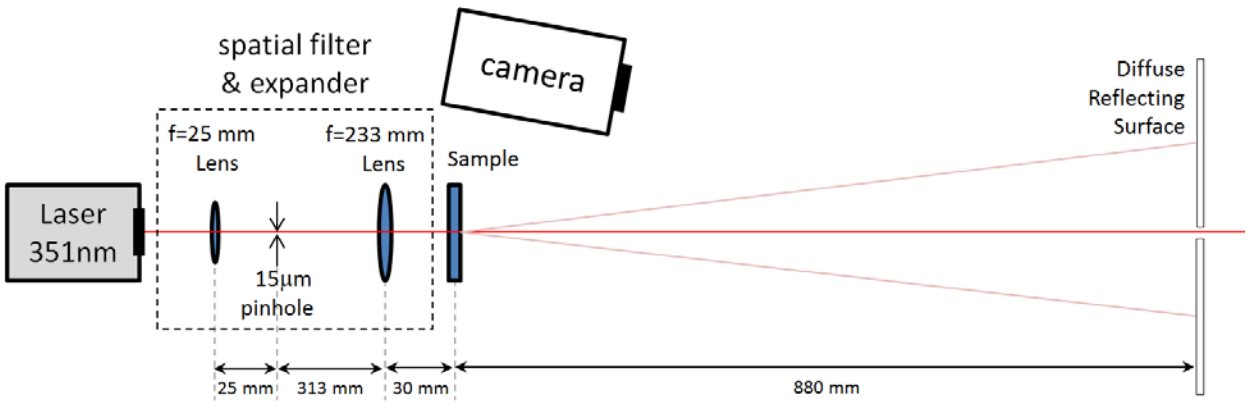


**Figure 1:** Scattered power and irradiation experimental setup layout: expanded and filtered ultraviolet laser beam (final f#~45) is passed through the sample and then incident on a

diffuse screen at far-field, which is imaged by programmable high speed electronic shutter CCD camera.

Post-processing of the images is used in order to subtract the background and average out the noise. The background is measured by taking the same measurement without the sample and is then subtracted from the measurement with the sample. The main two noticeable background artifacts are bias base level and scattering around the perforation at the screen center. For both cases with the sample (i.e., signal) and without it (i.e., background), 16 successive camera image frames have been averaged to reduce the noise level. Each frame is a result of integrated fluence over numerous camera electronic exposures (the number is varied between samples) of about 133 millisecond each. The laser repetition rate is set at about 10 KHz, therefore each image is an integration result of large number of laser pulses.

In order to normalize the scattered power by the beam total power, an additional measurement is taken imaging the entire beam reflecting of the surface. This measurement is performed without the sample and by shifting the diffuse screen such that the beam does not go through the perforation. Since the signal for this measurement is about 4 orders of magnitude higher than of that of the scattered power the camera is integrated over only one electronic camera exposure of much shorter exposure time (about half a millisecond). For this whole beam measurement the noise is also being averaged out using 16 successive frames and the bias background level to be offset is calculated from off-axis regions. The normalization of the signal (i.e., the background subtracted scatter) by the whole beam power is multiplied by the ratio in exposure time accordingly. The scattered irradiation and the integrated scattered power presented hereafter are reported as a fraction of the incident total power.

## 4. Comparison of model predictions and measured scattering from micro-machined pits

In order to validate the model predictions, we have fabricated a sample with a quasi-random ensemble of M-M shallow pits with similar dimensions using laser ablation (following the methodology detailed in [4,5]). Since the pit profiles are similar, the scatter of the ensemble is as that of the individual pits, which simplify the analysis and validation. The sample morphology is measured using 3D laser scanning confocal microscopy (VK-X100, Keyence Corporation, Elmwood Park, NJ), and the surface rendering of one of the shallow pits along with its height

profile are illustrated in Fig. 2 (a). Since the M-M pits are not Gaussian, their $\sigma_{eff}$ have to be evaluated based on their calculated volume ( $\sigma_{eff} = \sqrt{V/\pi h}$ ). A sample region containing 12 M-M pits was chosen, and the $\sigma_{eff}$ is depicted at Fig. 2(b), resulting in a mean value of 11.3 μm.

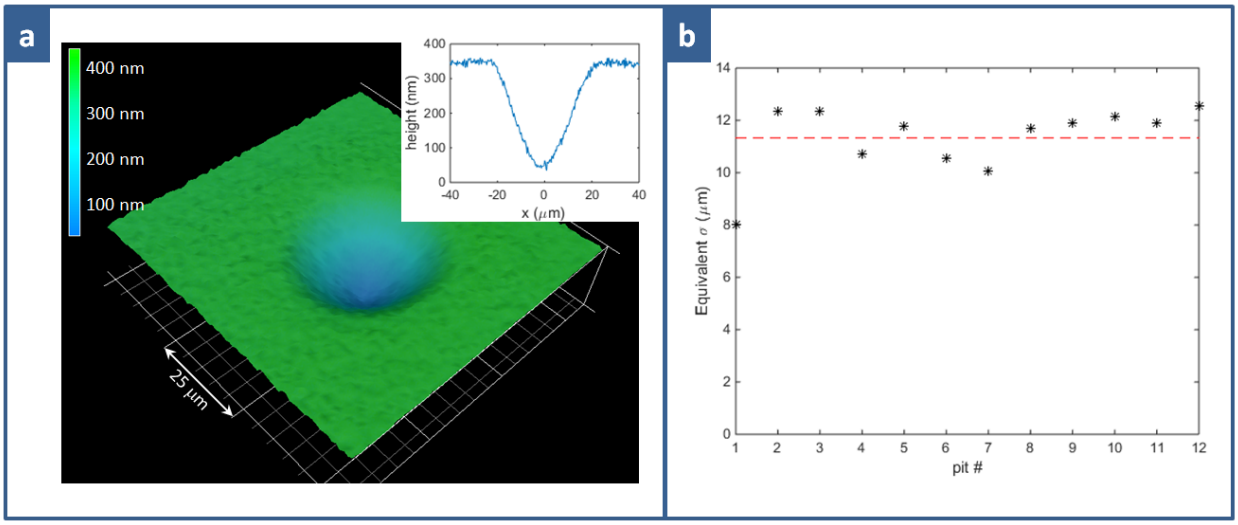


**Figure 2:** The morphology of precisely shaped M-M pits on silica substrate using laser ablation. (a) 3D rendering of typical shallow pit topology, with height profile view as inset. (b) Calculation of the equivalent $\sigma_{eff}$ for a segment containing 12 pits (mean value as red dashed line).

The measured scattering angle was found to be in excellent agreement with the predicted by the model. Based on the mean $\sigma_{eff}$ observed for the sample morphology and Eq. (2) the predicted scatter angle is: $\theta_{FF} \sim 0.351\mu m/(\pi \cdot 11.3\mu m) = 9.89 mrad$ . The measured scattered irradiance is depicted in Fig. 3 (a), obtained based on the methodology described in section 3 (here normalized to its pick value). The $\theta_{FF}$ refers to the angle at which the field magnitude decays to 1/e its value and the intensity to $1/e^2$ its value. At Fig. 3(a) the measured $\theta_{FF}$ ~10 mrad, observed at $1/e^2$ of the maximal value, which matches the predicted value.

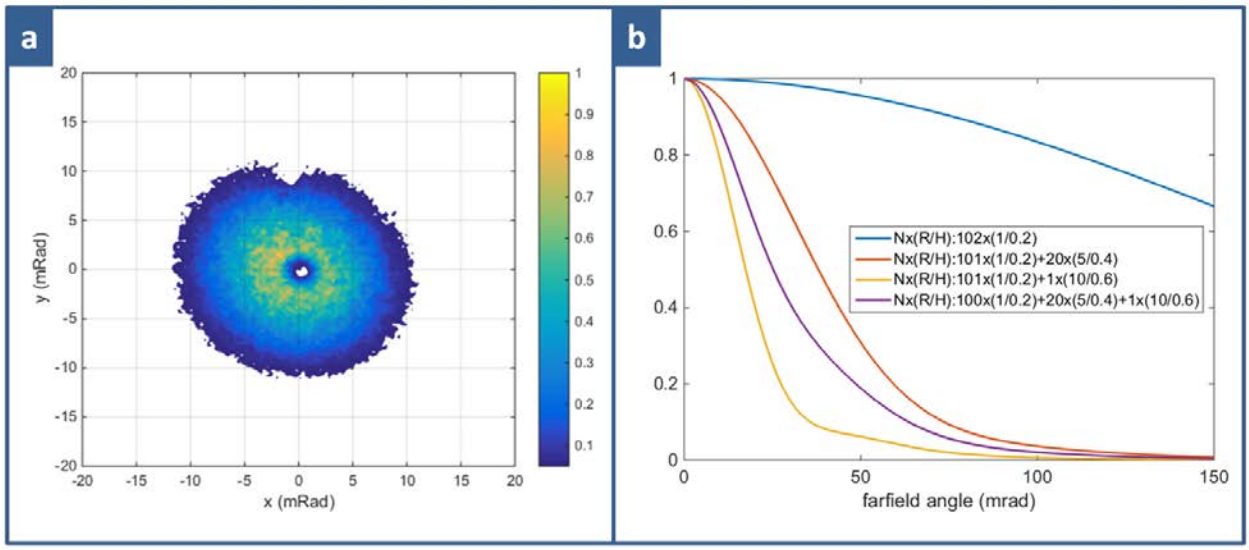


**Figure 3:** (a) Measured scattered irradiation from the M-M sample (described in Figure 2). The values are normalized to maximal value. (b) Calculation of designed scattered irradiation for different mixtures of shallow pits (the relative mixture of population is indicated as [number of pits] x ([pit radius] / [pit depth]), both dimensions are in microns).

The model prediction for the scattered power set a tight upper bound to the measured value. The scattered power based on Eq. (3) is: $P^{scat} = N \cdot (\eta \left| A_{NF} \right|^2) \cdot (\pi\sigma^2) \cdot \xi$ , where $N$ is the number of M-M pits in the area over which the calculation is done $S$. The incident power over this area is: $P = S \cdot (\eta \left| A_{NF} \right|^2)$ . Therefore the scattered power fraction of the beam is:

$$\frac{P^{scat}}{P} = \frac{N\pi\sigma^2}{S}\xi \qquad (5)$$

For the sample under evaluation, the average density of M-M pits is about 10 per mm$^2$ and the measured depth is 300 nm giving a cross-section of 2.7. Therefore the predicted scattered power is 1% of the total power. The measured scattered power is 0.75% of the total beam power, which is tightly bounded by the predicted value. The model prediction is expected to be slightly higher than the measurement, due to some small fraction of high-angles scattering that does not reach the far-field [6].

This measurement validates the model as well as demonstrating that carefully designed scattering plates could be tailored to a desired scatter profile. To further illustrate this capability we have simulated few scatter profiles based on different compositions of shallow pits

populations of different sizes. The four curves in Fig. 3(b) are of the far-field scattered irradiance (normalized to its maximum value) for the four relative compositions, where the radius (defined as 3 times $\sigma$ of the Gaussian) and depth of the Gaussian shaped pits are given at the legend. The scatter irradiance of homogenous ensemble of h=200 nm Gaussian pits with R = 1 μm radius (blue curve) is shown to be very broad (>>150 mrad). As the composition of the ensemble is changed to be a mixture of about one larger pit (R=5 μm, h=400 nm) for every five pits as before, the scatter irradiation narrows substantially to about 70 mrad (red curve). Replacing the larger pit in the composition to be even larger (R=10 μm, h=600 nm) further narrows the scatter angle to 30 mrad (yellow curve). Finally, mixing the three types of pits in a ratio of 100: 20:1 (smallest : medium : largest) gives an intermediate curve (purple curve) with scatter angle of about 55 mrad.

## 5. Scattering from laser-induced shallow pits derived from surface bound particles

After validating the scattered power measurement setup with the model, we now turn to study the scattering when the beam is incident on pitted exit surface of silica glass samples – representative of metal particle laser ablation. The samples were prepared by sprinkling 20 μm diameter spherical aluminum particles on the exit surface of 4 silica slabs (this procedure is further detailed in [9]), after surface cleaning and HF-etching (see details in [3]). Each sample has been exposed to a large aperture (~ 3 cm) 5 ns pulsed laser at the ultraviolet (λ=351 nm) at a different fluence [14]: 2 J/cm$^2$, 5 J/cm$^2$, 8 J/cm$^2$, and 11 J/cm$^2$. The morphology of the surface has been characterized using confocal laser scanning microscope. A scan area of 2.5 mm x 2.5 mm has been stitched together from multiple high resolution sub scans at lateral resolution of 0.5 μm per pixel and depth resolution of 0.1 nm per vertical pixel, and linear tilt has been corrected. The height maps of representative segments at the four samples are presented at Fig. 4 (a), where black regions indicate depressions in the surface. This collected data supports that increasing the laser exposure enhances the amount of pitting, and also shows that at the low fluence sample a larger number of bound particles have been remained. The underlying mechanisms resulting in the creation of the LSPs as well as a more detailed structural parameter study are outside the scope of this work and will be discussed elsewhere.

To better characterize the dimensions of the LSPs on the four samples we have processed the image resulting in a list of the width and depth of the measured surface depressions. Image processing was conducted to threshold the image (ImageJ, National institutes of Health, USA) to find the depressions in the sample and particle analysis to characterize the dimensions of the detected segments. To enhance the statistics we have included two 2.5 mm x 2.5 mm scanned segments per sample. The results are depicted in Fig. 4 (b) on a log-log scale. Only on the 11 J/cm$^2$ sample damage sites (classified as a type III in [14]) have been detected. The two detected laser damage sites are indicated in Fig. 4 (b) by 'A', and clearly appear in Fig. 4 (a) as the two large irregularly shaped black regions. The morphology of one of these sites is further illustrated in Fig. 4 (b) by the false color 3-D rendering labeled accordingly by 'A'. The other type of laser induced features found much more abundantly on the surface are the LSPs, indicted by 'B', 'C', and 'D'. These axisymmetric, Gaussian-like profiles are the main focus of this paper and appear as single LSPs for the fluences of 8 J/cm$^2$ and below (indicated by 'B'), and in the high fluence shot also in bunches of LSPs spaced by linear-like groove (indicated by 'C' and 'D'). The last set of features detected is particles that have not been cleaned by the laser, indicated by 'E'.

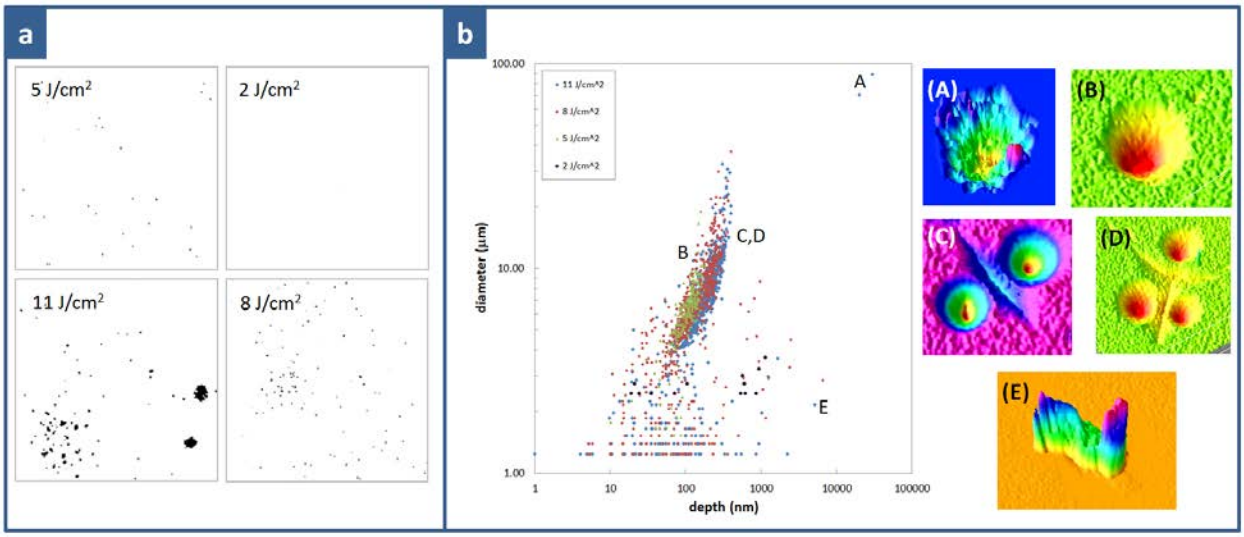


**Figure 4:** The morphology of the silica sample exit surface pitting induced by laser cleaning of metal micro-particle: (a) height maps of the representative segments at the four samples (1.25 mm x 1.25 mm) induced by different fluences indicated on the image (black indicates depression). (b) Pit dimension analysis of the detected pits population for the 4 samples, along with 3D height rendering of typical artifacts (indicted by 'A' – 'E' letters).

Based on the morphology characteristics described in Fig. 4, the power scatter predicted by the model fits well the observations from the scatter measurement. The scatter measurements for

the four samples are shown in Fig. 5. The irradiance of the highest fluence sample is displayed in Fig. 5 (a), and a one-dimension profile is displayed in Fig. 5 (b), along with the complementary results for the other samples. It is immediately clear that the scatter increase as the sample was exposed to higher fluence, as expected due to deeper pitting. The values of the total scattered power are shown in the legend of Fig. 5 (b) and follow the same trend. On the 2 J/cm$^2$ sample only a small amount of existing particles where detected, and the scattered power level detected is very small having almost flat irradiance – at the measurement noise level. As the laser fluence is increased, the population of detected LSPs has higher diameter and depth – expected to result in a higher scattered power from the LSPs population. The diameter of the dominant LSPs for the 11 J/cm$^2$ sample is about 30 μm, which translates based on Eq. (2) to an expected scatter angle of about 20 mrad – which fits the measurement in Fig. 5 (b) (see the dashed line indicated by (B)). For the 8 J/cm$^2$ case, the LSPs diameter is similar but the depth is slightly smaller, and as observed in Fig. 5 (b), the resulting scatter is lower in magnitude but has similar scatter angle. For the 5 J/cm$^2$ sample the dominant LSPs diameter is about 10 μm and also smaller in depth and number of counts, and therefore expected to have smaller magnitude of scatter and a broader angle. The magnitude reduction is clearly observed in the measurement. However, even though a small broadening could be observed in the scatter irradiation curve, it is hard to examine the broadening since the measured signal is reaching at these scatter angles close to the measurement noise level. Finally, the two detected laser damage sites (indicated by 'A') for the 11 J/cm$^2$ sample have very large volumes and therefore are expected to result in a large scatter contribution for this sample. Since their diameter is about 100 μm, they are expected to yield an additional feature of few mrad scatter angle as clearly seen in Fig. 5 (b) (see the dashed line indicated by (A)). The clear correlation made by the model between the scattered power measurements to the sample morphology, indicates also that analysis of the scatter irradiance based on the model could serve as a method indicating the presence of scattering features on samples. For example, detection of the few milli-radians features in the scatter irradiance would indicate the presence of laser damage sites presence.

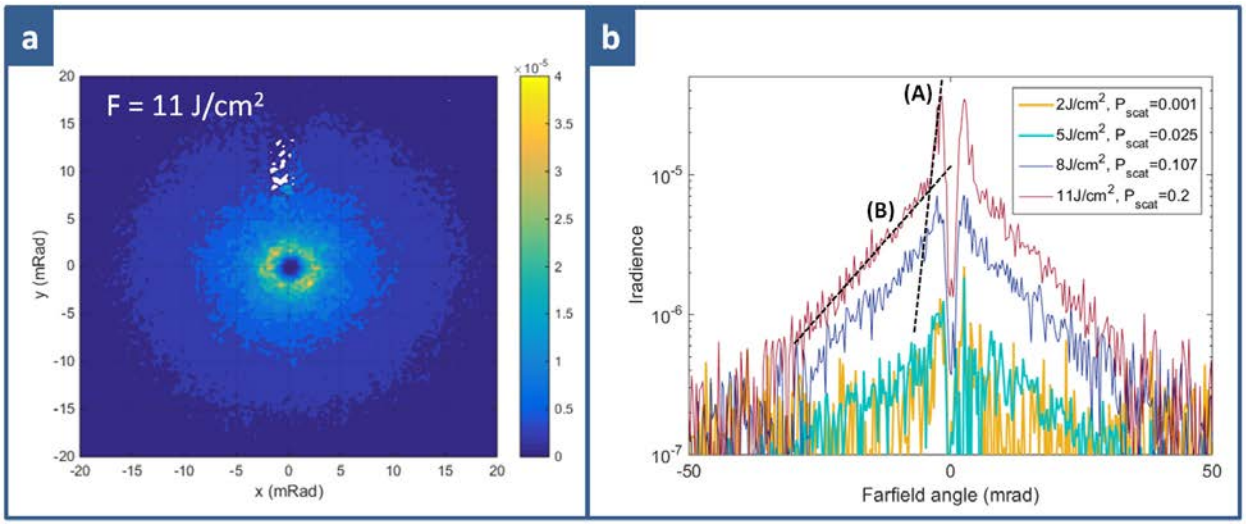


**Figure 5:** Scatter irradiation of the four samples with exit surface pitting induced by laser cleaning, and characterized in Figure 4: (a) the 2D irradiance of the sample with exposure fluence of 11 J/cm$^2$. The scattered power is normalized as a fraction of the incident beam power. (b) Profile of the irradiance (through the x-axis) for the four samples. The scattered power as a fraction of the incident beam power is given at the legend. The dashed lines illustrate the different contributions of Fig. 4 object types (A) and (B) to the 11J/cm$^2$ curve.

## 6. Conclusions

We have experimentally validated a model that ties the morphology features of laser-induced shallow pits at the exits surface of silica slab to the scattered power and irradiation of a beam that passes through the sample. The model predictions are in excellent agreement to the measurement for the precise profile micro-machined shallow pits. With the use of this model and a carefully designed mixture of shallow pits a tailored scatter irradiation plate could be fabricated. Using the same methodology as for micro-machined samples, scattering resulting from pitting caused by laser cleaning of bound metal micro-particles at different fluences, show good agreement with the model predictions. The total off-axis scattering from the samples increases with increasing laser fluence. The model allows inference from the observed features in the irradiation measurement about the morphology and the types of scattering object present on the sample.

## Acknowledgements

We would like to acknowledge Gabe Guss for preparing the designed sample described in Fig. 2, and to acknowledge Rajesh Raman and the optical sciences laboratory (OSL) staff for preparing the laser cleaning samples described in Fig. 4.

This work was performed under the auspices of the U.S. Department of Energy by Lawrence Livermore National Laboratory under contract DE-AC52-07NA27344. We would like to acknowledge the funding from Laboratory Directed Research and Development grant 14-ERD-098.

## References

1 S. G. Demos, M. Staggs, K. Minoshima, J. Fujimoto, "Characterization of laser induced damage sites in optical components," Opt. Express 10, 1444-1450 (2002).

2 B. Bertussi, P. Cormont, S. Palmier, P. Legros, J. Rullier, "Initiation of laser-induced damage sites in fused silica optical components," Opt. Express 17, 11469-11479 (2009).

3 T. I. Suratwala, P. E. Miller, J. D. Bude, W. A. Steele, N. Shen, M. V. Monticelli, M. D. Feit, T. A. Laurence, M. A. Norton, C. W. Carr, L. L. Wong "HF-based etching processes for improving laser damage resistance of fused Silica optical surfaces," J. Am. Ceram. Soc. 94, 416–428 (2011).

4 I. L. Bass, G. M. Guss, M. J. Nostrand, P. L. Wegner, "An improved method of mitigating laser-induced surface damage growth in fused Silica using a rastered, pulsed CO2 laser", Proc. SPIE 7842, Laser-Induced Damage in Optical Materials: 2010, 784220

5 M.J. Matthews, S.T. Yang, N. Shen, S. Elhadj, R.N. Raman, G. Guss, I.L. Bass, M.C. Nostrand, P.J. Wegner, "Micro-Shaping, Polishing, and Damage Repair of Fused Silica Surfaces Using Focused Infrared Laser Beams," Advanced Engineering Materials 17, 247-252 (2015)

6 E. Feigenbaum, S. Elhadj, M.J. Matthews, "Light scattering from laser induced pit ensembles on high power laser optics," Opt. Express 23, 10589-10597 (2015).

7 S. Palmier, I. Tovena, L. Lamaignère, J. L. Rullier, J. Capoulade, B. Bertussi, J. Y. Natoli, L. Servant, "Study of laser interaction with aluminum contaminant on fused silica," Laser-Induced Damage in Optical Materials 2005, Proc. of SPIE Vol. 5991 59910R

8 B.S. Luk`yanchuck, *Laser Cleaning,* Chapter 3, (World Scientific, 2002)

9 M.J. Matthews, N. Shen, J. Honig, J.D. Bude, A.M. Rubenchik, “Phase modulation and morphological evolution associated with surface-bound particle ablation,” J. Opt. Soc. Am. B 30, 3233 (2013)

10 L. N. Deepak Kallepalli, D. Grojo, L. Charmasson, P. Delaporte, O. Utéza, A. Merlen, A. Sangar, P. Torchio, “Long range nanostructuring of silicon surfaces by photonic nanojets from microsphere Langmuir films,” J. Phys. D: Appl. Phys. 46, 145102 (2013).

11 H. C. van de Hulst, Light Scattering by Small Particles (Dover, NY, 1981)

12 J. C. Stover, Optical Scattering: Measurement and Analysis, Third Edition (SPIE, 2012)

13 T. A. Germer, C. C. Asmail, “Polarization of Light Scattered by Microrough Surfaces and Subsurface Defects,” J. Opt. Soc. Am. A 16, 1326-1332 (1999)

14 M. C. Nostrand, T. L. Weiland, R. L. Luthi, J. L. Vickers, W. D. Sell, J. A. Stanley, J. Honig, J. Auerbach, R. P. Hackel, P. J. Wegner, “A large aperture, high energy laser system for optics and optical component testing,” Proc. SPIE 5273, 325–333 (2003)

15 R.A. Negres, D.A. Cross, Z.M. Liao, M.J. Matthews, C.W. Carr, ” Growth model for laser-induced damage on the exit surface of fused silica under UV, ns laser irradiation,” Opt. Express 22, 3824-3844 (2014)